Applied Physics Letters

Probing lattice dynamics in ST12 phase germanium nanowires by Raman spectroscopy

Cite as: Appl. Phys. Lett. **119**, 232105 (2021); https://doi.org/10.1063/5.0066744
Submitted: 12 August 2021 • Accepted: 17 November 2021 • Published Online: 08 December 2021

Sreyan Raha, Divya Srivastava, Subhajit Biswas, et al.

Applied Physics Letters ARTICLE scitation.org/journal/apl

Probing lattice dynamics in ST12 phase germanium nanowires by Raman spectroscopy

Cite as: Appl. Phys. Lett. **119**, 232105 (2021); doi: 10.1063/5.0066744
Submitted: 12 August 2021 · Accepted: 17 November 2021 ·
Published Online: 8 December 2021

Sreyan Raha,[1] Divya Srivastava,[2] Subhajit Biswas,[3] Adrià Garcia-Gil,[3] Antti J. Karttunen,[2] Justin D. Holmes,[3] and Achintya Singha[1,a)]

AFFILIATIONS

[1]Department of Physics, Bose Institute, 93/1 Acharya Prafulla Chandra road, Kolkata 700009, India
[2]Department of Chemistry and Materials Science, Aalto University, P.O. Box 16100, FI-00076 Aalto, Finland
[3]School of Chemistry & Advanced Materials and Bioengineering Research (AMBER) Centre, University College Cork, Cork T12 YN60, Ireland

[a)]Author to whom correspondence should be addressed: achintya@jcbose.ac.in

ABSTRACT

Germanium (Ge) plays a crucial role in setting up important functionalities for silicon-compatible photonics. Diamond cubic germanium is an extensively studied semiconductor, although its other exotic forms, like BC8, ST8, ST12 phases, may possess distinct electronic properties. We have fabricated stable ST12-Ge nanowires via a self-seeded bottom-up three phase growth in a confined supercritical toluene environment. Here, we report on the direct evidence of the presence of the ST12 phase by a combination of Raman spectroscopy and first-principles calculations using density functional theory (DFT). It is important to remark that the DFT calculation predicts all the Raman active optical phonon modes of the P 4_32_1 structure, and it is in very good agreement with the experimental results. The phonon dynamics as a function of temperature is investigated through Raman measurements at temperatures varying from 80 to 300 K. First-order temperature coefficients for all the observed Raman modes are estimated from the linear temperature dependence of the phonon shifts. A complete set of isobaric Grüneisen parameters is reported for all Raman modes of ST12-Ge nanowire, and the values are lower compared to the same for Si, dc-Ge bulk, and Ge nanowire. These results have important implications for understanding thermal properties of ST12-Ge nanowire.

Group IV elements have drawn great attention because of their potential applications in present-day consumables and devices.[1–6] Germanium (Ge) is one of the widely used group IV materials for the development of photonics, nanoelectronics, and optoelectronics.[7–10] Though the diamond cubic (dc) Ge is mostly studied and used, Ge can also be found in some other exotic forms, which are potentially very useful in photovoltaics, transistors, and superconducting devices.[11–14] These phases can be procured on the suitable tuning of thermodynamic condition especially pressure.[15] However, most of the phases are metastable and can only be realized under a definite decompression condition of compressed Ge.[16–22] Under pressure, dc-Ge undergoes a series of transformations. At 10–11 GPa, it converts into metallic $\beta-$Sn Ge, which transforms into the orthorhombic Imma phase around 75 GPa and then simple hexagonal structure around 90 GPa.[23–25] Around 100 GPa, it transforms to a Cmma phase, which changes into the hcp structure around 160–180 GPa. When hcp Ge is decompressed, it does not follow its previous path. Moreover, it forms various allotropes depending on the rate of pressure release. It is reported that on decompression, Ge can take various structures, such as BC8, R8, and ST12.[24,26–29] The $\beta-$Sn phase readily transforms into the BC8 phase and then hexagonal Ge on very fast release of pressure,[16,25,28,30] while slow decompression results in the metastable ST12 structure.[17,18,31] Some reports also suggest that metallic amorphous Ge, formed by pressure, can be transformed to both BC8[16,19,29] and ST12 phase[20] on depressurization.

Among all the Ge allotropes, ST12 is kinetically more stable at ambient conditions. It contains 12 atoms per unit cell in the space group P 4_32_12 (D_4^8)[32] and possess distorted tetrahedral arrangement with atoms placed in fivefold, sixfold, and sevenfold rings.[32,33] Thus, the electronic property of the ST-12 Ge is expected to be semiconducting and can be also realized as a superconductor at low temperature by doping.[13,14] Moreover, due to the stronger binding interaction of Li atoms within the ST12 Ge lattices, it shows higher Li intercalation compared to the dc-Ge and demonstrates as a promising candidate for energy storage applications.[11] Theoretical and experimental efforts have been devoted to explore the electronic band structure and

thermal stability of the ST12-Ge.[13,31,34,35] However, studies on lattice dynamics, which is responsible for thermal properties of a material, are limited. Malone and Cohen have calculated phonon dispersions for bulk ST12-Ge using local density approximation (LDA).[13] Raman scattering is among the most conventional and fundamental techniques for studying lattice dynamics of materials in an easy and nondestructive manner. The structural and vibrational properties of the various phases of Ge under pressure have been studied using Raman spectroscopy. Very recently, Zhao *et al.* reported optical phonon modes of bulk ST12-Ge via Raman analysis and calculation.[32] The reported results, however, are limited to the bulk system, and no one has observed all the Raman active optical modes of the ST12-Ge crystal. Downscaling the dimension of ST12-Ge to a nanometer regime may lead to potential functionality and device concepts. We are aware of few reports on nanocrystalline ST12-Ge fabricated through thermal annealing of amorphous nanoscale Ge[36] and evaporation.[37,38] However, no one synthesized the quasi one-dimensional nanostructures, which are used as the building blocks for several technologies including electronics,[39] optoelectronics,[1,2] energy storage device,[3,4,40,41] and sensor.[5,6,42,43]

Here, we demonstrate the synthesis of ST12-Ge nanowires (NWs). The phase and purity of the NW are confirmed from x-ray diffraction (XRD) and high-resolution transmission electron microscopy (HRTEM). We have conducted a systematic Raman study and observed almost all the Raman-active optical phonon modes. Density functional theory (DFT) calculations were also performed. Combining calculated Raman frequencies and their intensity with the experimental results enable us to clearly identify all the observed modes. Finally, temperature dependent Raman measurements have been performed on ST-12 Ge, allowing us to estimate first-order temperature coefficients and isobaric Grüneisen parameters.

The ST12-Ge NW synthesis procedure and the methods used for characterization are given in the supplementary material. Figures 1(a) and 1(b) show representative low magnification SEM image and high magnification TEM image of ST12-Ge NWs. (Methods used for characterization can be found in the supplementary material.) Figure 1(a) exhibits the formation of high yield of reticulated NWs, which are several micrometers long. Ge NWs assembled together to form a uniform continuous Ge film over the Si substrates. SEM analysis become limited for accurate estimation of the morphological quality of the NW and the NW surface due to the reticulation of the NWs. Thus, detailed morphological analysis of the NWs is performed via TEM. The presence of an amorphous carbonaceous structures can be spotted along the Ge NW as an uneven coating [Fig. 1(b)]. The formation of the carbonaceous structure was confirmed via x-ray photoelectron spectroscopy (XPS), with the presence of Ge–C, C–C, C=C, C–O, and CO_3 bonds in the C1s spectrum (see Fig. S1 in the supplementary material). The formation of the carbonaceous compound is aided by the decomposition of the Ge precursor (DPG) to form Ge adatoms and liberating very reactive phenyl groups.[44] The *in situ* formation of Ge nanoparticle seed and the carbonaceous compound on NW surface, and its interaction with the Ge is a key for the formation of the ST-12 NW

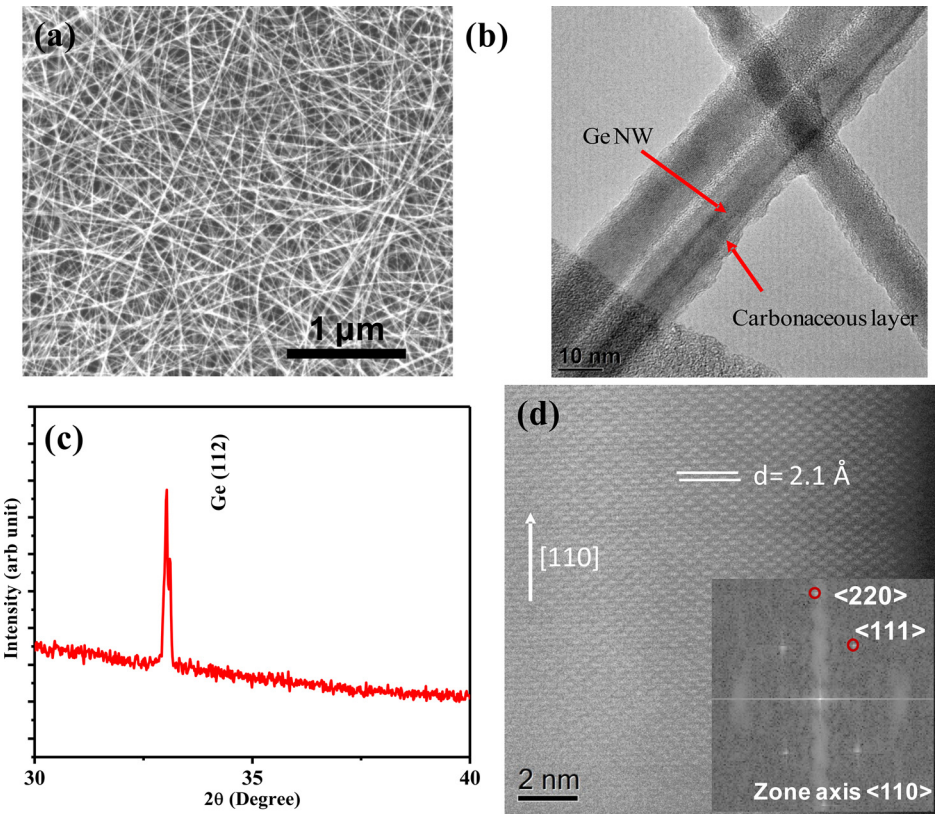

FIG. 1. (a) SEM micrographs of ST12-Ge NW. (b) Low magnification TEM image showing the uniform diameter nanowire formation with amorphous shell. (c) XRD pattern of the nanowire sample showing a ST12-Ge crystal structure obtained after subtracting the Si (100) substrate peaks. (d) Latticed-resolved HRTEM image and corresponding FFT (in the inset) of ST12-Ge nanowires.

structure. We have delegated details of the growth mechanism of ST12-Ge NW to a different study as this paper is primarily focused on the Raman analysis of these structures. The diameter of Ge NWs was found to be uniform with an average diameter of 9.0 (± 1.4) nm.

XRD on the as-grown NW was performed to confirm the crystal structure and the phase purity of the NWs [Fig. 1(c)]. The pattern shows a sharp peak at 2θ of 33.29°, after subtracting the reflection peaks from the Si pattern of the substrate. The XRD pattern matches well with the calculated and experimental XRD pattern of ST12-Ge (JCPDS No. 72–1089, $a = 5.93$ Å, and $c = 6.98$ Å).[45,46] We have assigned the peak in the XRD pattern to the reflection from the (112) plane as this is the closest match with the 2θ value. Peaks corresponding to dc-Ge were not observed in the XRD pattern. The single peak observed in the XRD corresponds to the strongest (112) reflection from the ST-12 Ge sample and associated with the crystallographic orientation of the one-dimensional NW. Due to the bulk crystalline nature of the sample, Zhao *et al.* have observed several diffraction peaks in their powder x-ray diffraction (PXRD) data associated with the different lattice planes of the ST-12 crystal.[32] HRTEM and Fast Fourier Transform (FFT) were used to further confirm the formation of ST12-Ge crystalline phase in the NWs and also verify the structural quality of the ST12-Ge NWs [Fig. 1(d)]. In general, NWs are single crystalline and free of any crystalline defects such as twin boundaries and stacking faults. HRTEM image recorded with ⟨110⟩ zone axis alignment reveals an interplanar spacing (d) of 0.21 nm corresponding to the (220) plane of the ST12-Ge crystal structure (JCPDS No. 72–1089). A hexagonal symmetry was observed in the FFT pattern where the spots are associated with the (111) and (220) planes [inset of Fig. 1(d)] where ⟨110⟩ is the growth direction of the ST12-Ge NW. The Selected Area Electron Diffraction (SAED) observed from the single crystalline bulk structure (in Zhao *et al.* paper[32]) shows multiple spot pattern from different crystalline planes. They have observed this from [310], [100], and [210] zone axis.

First-principles calculations using DFT have been performed to study the vibrational properties of both ST12-Ge and dc-Ge. The details of the computational method are given in the supplementary material. The DFT-Perdew–Burke–Ernzerhof [PBE0 is combination of the PBE (Perdrew-Burke-Ernzerhof) generalized gradient functional with a predefined amount of exact exchange.[47]]/triple-zeta valence with polarization (TZVP) optimized lattice parameters are $a = b = 5.92$ Å, $c = 7.03$ Å for ST12-Ge and $a = b = c = 5.70$ Å for dc-Ge, which are in good agreement with experimental lattice parameters $a = b = 5.93$ Å, $c = 6.98$ Å for ST12-Ge,[32] and $a = b = c = 5.66$ Å for dc,[47,48] respectively. For ST12-Ge, there are 36 vibrational modes observed. Among them, three are acoustic, and thirty-three are optical modes. The optical vibrational modes belong to the following irreducible representations: $\Gamma_{vib} = 4A_1 + 4A_2 + 5B_1 + 4B_2 + 8E$. A_1 and B_2 are totally symmetric and totally anti-symmetric phonon modes, respectively. E is doubly degenerate phonon modes. A_2 (B_1) is symmetric (anti-symmetric) with respect to principal axis of symmetry and anti-symmetric (symmetric) with respect to a C_2 axis. The modes A_2 and E are infrared-active mode, whereas A_1, B_1, B_2, and E are Raman-active modes. Our DFT calculations predict 21 ($4A_1 + 5B_1 + 4B_2 + 8E$) Raman active optical modes, which is in accordance with group theoretical analysis of the P 4_32_1 structure[32] and previously reported DFT calculations.[13] This agreement is consequence of imposing space group constrain on the crystal structure during optimization. The Raman frequency and the symmetry of the modes estimated from the calculation are presented in the second column of Table I. For comparison, we have calculated Raman spectrum of dc-Ge, which shows that the Raman active mode (E_{2g}) originates from a degenerate LO–TO phonon mode (see Fig. S2 in the supplementary material).

TABLE I. Calculated Raman frequency and symmetry of ST12-Ge, measured Raman frequency of ST12-Ge NW, reported (experimental) Raman modes of ST12-Ge from other works, first-order temperature co-efficient (β) and isobaric mode Grüneisen parameter (γ_{ip}).

Peak number	Calculated Raman frequency (cm^{-1}) and symmetry of ST12-Ge	Experimentally measured Raman frequency (cm^{-1})	Reported Raman frequency of ST12-Ge from Zhao *et al.*[32] (cm^{-1})	β_i (cm^{-1} K^{-1})	$\gamma_{ip} = -\frac{1}{\alpha\omega_i}\beta_i$
1	66.1 (B_1)	65 (±2)	55	−0.001 07 (±0.000 49)	0.39 (±0.19)
2	90.5 (E)	84 (±3)	85, 90	−0.006 81 (±0.000 71)	1.90 (±0.30)
3	96.9 (A_1), 101.3 (E)	93 (±3)	100	−0.000 52 (±0.000 23)	0.13 (±0.06)
4	102.0 (B_2), 104.5 (B_1)	100 (±3)		−0.002 56 (±0.000 34)	0.60 (±0.10)
5	113.2 (A_1)	116 (±3)		−0.003 33 (±0.000 51)	0.68 (±0.13)
6	166.5 (E)	155 (±5)		−0.023 28 (±0.009 21)	3.56 (±1.49)
7	196.1 (E)	183 (±5)	190	−0.021 59 (±0.002 63)	2.80 (±0.49)
8	199.5 (A_1)	194 (±3)	200	−0.015 87 (±0.001 28)	1.93 (±0.20)
9	203.6 (B_2)	209 (±4)		−0.015 60 (±0.002 41)	1.77 (±0.33)
10	227.3 (B_1)	225 (±4)	210	−0.000 71 (±0.000 21)	0.07 (±0.02)
11	229.3 (B_2)	232 (±2)	230	−0.000 57 (±0.000 23)	0.05 (±0.02)
12	234.7 (E), 237.0 (B_1)	242 (±4)		−0.004 65 (±0.000 25)	0.45 (±0.03)
13	254.5 (E)	261 (±4)	257	−0.008 86 (±0.000 11)	0.81 (±0.02)
14	282.7 (E), 285.4 (A_1)	275 (±5)	275	−0.011 71 (±0.006 02)	1.01 (±0.07)
15	291.3 (E)	289 (±3)		−0.012 88 (±0.001 91)	1.06 (±0.16)
16	297.5 (B_1)	300 (±4)		−0.014 27 (±0.006 07)	1.12 (±0.49)
17	305.7 (B_2)	307 (±3)		−0.017 56 (±0.002 27)	1.35 (±0.18)

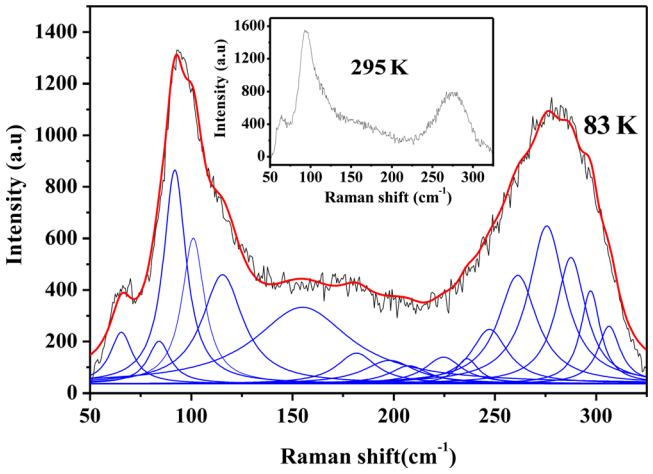

FIG. 2. Deconvoluted Raman spectrum of ST12-Ge NW measured at 83 K fitted with 17 Lorentzian functions. Inset shows the Raman spectrum of ST12-Ge NW at 295 K.

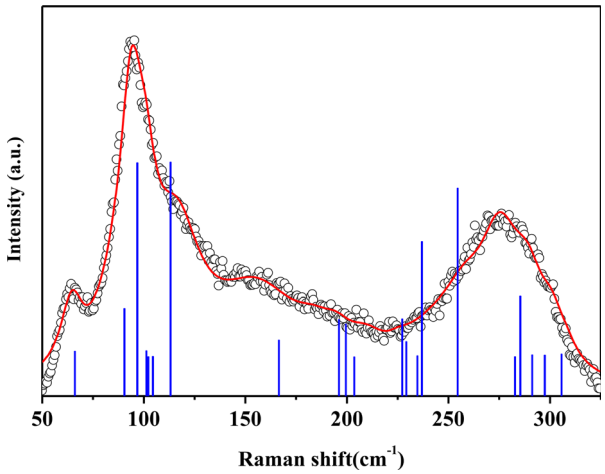

FIG. 3. Experimental Raman spectrum of ST12-Ge NW and calculated Raman modes (blue bars) with undefined FWHMs. Height of each bar is the measure of intensity of corresponding Raman mode.

Figure 2 displays a typical Raman spectrum in 50–325 cm^{-1} range measured from the ST12-Ge NW sample at 83 K. A similar Raman spectrum measured from the same NW sample at room temperature is shown in the inset of Fig. 2. Both the spectra show identical line shapes. However, a better resolution is observed in the spectrum recorded at low temperature. In ST12-Ge NWs with average diameter ~9 nm, the quantum confinement effect is very obvious. The confinement of phonon relaxes the $q = 0$ selection rule in the Raman scattering and results in the change in phonon mode frequency and linewidth broadening. Moreover, the scattering of phonon in the low dimensional system provided additional linewidth broadening. Therefore, the Raman spectra are broad in the present work compared to the data reported by Zhao *et al.*[32] Analysis of the spectra was performed very carefully. Out of 21 predicted modes from DFT calculation some modes are extremely weak and closely spaced [96.9 cm^{-1} (A1) and 101.3 cm^{-1} (E), 102.0 cm^{-1} (B2), and 104.5 cm^{-1} (B1), 234.7 cm^{-1} (E) and 237.0 cm^{-1} (B1), 282.7 cm^{-1} (E), and 285.4 cm^{-1} (A1)]. Thus, for deconvolution of the spectrum, we consider a single peak at the average position of two closely positioned weak peaks. Therefore, to fit the experimental spectra, we have used 17 modes with the peak position, intensity, and width as free fitting parameters. The reference values of peak position are taken from the DFT calculation. The experimental spectrum is nicely fitted with 17 Lorentzian line shapes. The fitted data in the range 50–325 cm^{-1} are displayed in Fig. 2, and their positions are presented in Table I. To obtain the error in the fitting, we fit the spectrum five times and estimated error for peak position, which are given in Table I.

Out of 17 observed Raman modes for ST12-Ge NWs, only some are previously reported[32] (see Table I). In this report of Raman analysis on ST12-Ge NW, the calculated Raman spectrum is almost fully matched with the experimental spectrum. The calculated intensities of the Raman modes also match nicely with the intensity pattern of the experimental spectrum as displayed in Fig. 3, further adding credibility to our mode assignment.

To get the information about the Raman selection rule, polarized Raman spectroscopy was performed on a single ST12 Ge NW transferred on a substrate. The measurements were performed in backscattering geometry. The light is incident on the NW along z-direction and scattered along the $\bar{z}$-direction. The polarization of the incident light lies in the xy plane. The experiment was carried out in two different configurations. According to the Porto notation, the Raman spectra are marked as $z(x,x)\bar{z}$ where the polarization of the incident and scattered light both are parallel to the x axis and $z(x,y)\bar{z}$ where the polarization of the incident and scattered light are in crossed polarization configuration. We have divided the measured spectra into two segments (Fig. 4). The modes below 125 cm^{-1} show strong polarization sensitivity, but the modes above 125 cm^{-1} exhibit nearly polarization-independent behavior. The modes at 66 cm^{-1} (B_1) and 90.5 cm^{-1} (E) are allowed in a crossed polarization configuration $[z(x,y)\bar{z}]$, whereas the modes around 100 cm^{-1} [(A_1) and (E)] and 102 cm^{-1}[(B_1) and (B_2)] are week in the $z(x,y)\bar{z}$ configuration, and become stronger in $z(x,x)\bar{z}$ scattering geometry.

Furthermore, to get greater insight into lattice dynamics, we have performed temperature dependent Raman study between 80 and 300 K. Raman spectra measured at different temperatures are shown in Fig. 5(a). For a more accurate analysis of the temperature-dependent Raman results, we have fitted the spectra with the Lorentzian functions. The estimated peak positions, which are plotted as a function of temperature, are shown in Fig. 5(b). All the ST12-Ge phonon modes show a redshift with the increase in the temperature. The Raman peak shift with temperature is mainly caused by the anharmonic phonon–phonon interaction and thermal expansion. In order to analyze the temperature dependent phonon softening, we have used a simplified phonon decay model, originated from Balkanski's approach,[49]

$$\omega_T = \omega_0 + \beta T, \tag{1}$$

where ω_0 is the Raman frequency at 0 K and β is the first-order temperature coefficient. In this model, the higher-order temperature coefficients have not been taken into account as they are not significant in the studied temperature range.

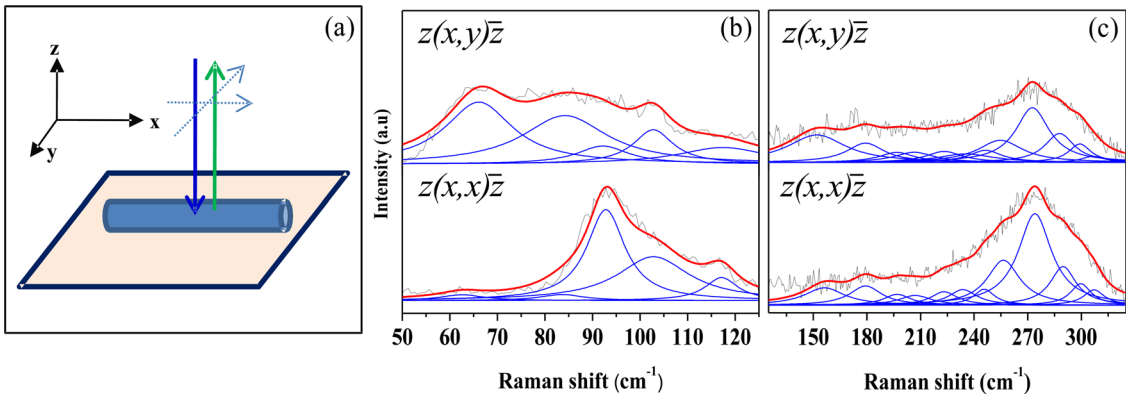

FIG. 4. (a) Illustration of the scattering geometry for polarized Raman measurements. Light is incident and scattered along z and $\bar{z}$ axes, respectively. The polarization of the light lies in the xy plane. (b) and (c) Deconvoluted Raman spectra for two polarization configurations as labeled in the figure ranging from 50 to 125 and 125 to 325 cm^{-1}, respectively.

We fitted the experimental result with the expression (1), and the obtained values of β are given in Table I. The β value for dc-Ge NW ($-0.0147\,cm^{-1}\,K^{-1}$) has also been estimated from the data presented in Fig. S4 (see the supplementary material), and it is in good agreement with the previous work.[50] The estimated β values for most of the Raman modes of ST12-Ge are lower than the same for dc-Ge. The observed differences in the β indicate that phonon anharmonicity caused by the scattering is lower in the ST12-Ge NW compared to the dc-Ge NW.[51]

Grüneisen parameter (γ) is an important thermo elastic value of solid, which describes the changes in unit cell volume caused by temperature and pressure. This parameter relates the property of a material to its vibrational energy and indicates the anharmonic effects on the phonon spectrum under temperature and pressure. The isobaric mode Grüneisen parameter (γ_{ip}) is related to the β by means of the following equation:[52]

$$\gamma_{ip} = -\frac{1}{\alpha\omega_i}\beta_i, \tag{2}$$

where ω_i is the Raman frequency of the i_{th} phonon mode and α is the thermal expansion coefficient.

To calculate γ_{ip}, we have taken the value of α for ST12-Ge from Ref. 53. Using Eq. (2), a complete set of γ_{ip} calculated from experimentally obtained β_i values for the entire observed optical phonon modes is reported in the last column of Table I. To compare the present results with the dc-Ge, we have estimated γ_{ip} for dc-Ge bulk and NW from the temperature dependent Raman data, which are presented in Figs. S3 and S4 in the supplementary material, respectively. The

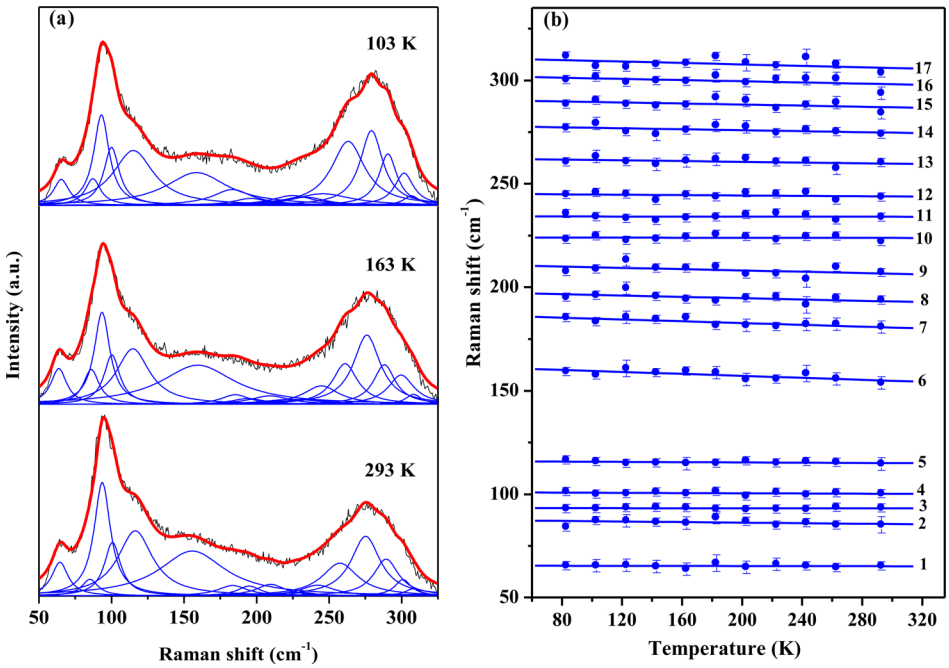

FIG. 5. (a) Raman spectra of ST12-Ge NW measured at 103, 163, and 293 K (scattered curves). The spectra are fitted with Lorentzian functions (blue curves). (b) Temperature dependence of the Raman peak position (scattered points) for all the observed modes. The solid lines represent the fit to Eq. (1).

obtained γ_{ip} for dc-Ge bulk and NW are 11.92 and 8.25, respectively, which are higher than the γ_{ip} of ST12-Ge NW (3.56). It is to be noted that the γ_{ip} values for both the NWs are lower than the same for bulk. With the decrease in the size of nanostructured materials, the bond length increases,[54] which reduces the lattice interaction and lowers the lattice vibration. As a result, less anharmonicity vibration gives lower values of the Grüneisen parameter.[55,56] High γ_{ip} value indicates lower thermal conductivity (k).[51] Hence, it is expected that the ST12-Ge NWs show low optical phonon scattering as well as high electrical and thermal conductivity compared to dc-Ge bulk and NW. Moreover, γ_{ip} values of the ST12-Ge are also lower than the γ_{ip} of silicon (7.00).[57] Therefore, the result implies that the ST12-Ge NW can be useful as a potential candidate for the thermal and electrical conductive material.

In summary, we have fabricated ST12-Ge NWs and confirmed the existence of this uncommon allotrope by XRD, HRTEM, and Raman study. In particular, we have performed detailed Raman spectroscopy and DFT analysis to pinpoint the ST12 phase of the nanostructure and to explore the phonon dynamics in this material. The experimentally measured Raman spectra are in agreement with the DFT calculations. Furthermore, the temperature dependent lattice dynamics of ST12-Ge NWs is investigated through temperature dependent Raman study. From the temperature dependent study, we have estimated first-order temperature coefficients and isobaric Grüneisen parameter for all the observed modes of ST12-Ge and the values are lower than the Si, dc-Ge bulk, and NW. Thus, our study not only provides the fundamental information that are important for technological applications of ST12-Ge but also attracts attention for further investigations on the role of dimension in polymorphism and in the thermal/vibrational properties of low-dimensional polymorphism of Ge, Si, and other semiconductors.

See the supplementary material for methods of nanowire synthesis, characterization, computational methods, XPS of ST12-Ge NW, calculated Raman spectrum of dc-Ge, and temperature dependent Raman study of bulk dc-Ge and dc-Ge NW.

The authors acknowledge financial support from Science and Engineering Research Board (SERB), India (File No. EMR/2017/002107). S.B., A.G., and J.D.H. acknowledge Science Foundation Ireland (Grant No. 14/IA/2513). Divya Srivastava would like to acknowledge CSC—the Finnish IT Center for Science for computational resources.

AUTHOR DECLARATIONS

Conflict of Interest

The authors have no conflicts to disclose.

DATA AVAILABILITY

The data that support the findings of this study are available from the corresponding author upon reasonable request.

REFERENCES

[1]P. Staudinger, M. Sistani, J. Greil, E. Bertagnolli, and A. Lugstein, "Ultrascaled germanium nanowires for highly sensitive photodetection at the quantum ballistic limit," Nano Lett. **18**, 5030–5035 (2018).
[2]L. N. Quan, J. Kang, C.-Z. Ning, and P. Yang, "Nanowires for photonics," Chem. Rev. **119**, 9153–9169 (2019).
[3]C. K. Chan, H. Peng, G. Liu, K. McIlwrath, X. F. Zhang, R. A. Huggins, and Y. Cui, "High-performance lithium battery anodes using silicon nanowires," Nat. Nanotechnol. **3**, 31–35 (2008).
[4]A. M. Chockla, K. C. Klavetter, C. B. Mullins, and B. A. Korgel, "Solution-grown germanium nanowire anodes for lithium-ion batteries," ACS Appl. Mater. Interfaces **4**, 4658–4664 (2012).
[5]N. Shehada, J. C. Cancill, J. S. Torrecilla, E. S. Pariente, G. Brönstrup, S. Christiansen, D. W. Johnson, M. Leja, M. P. A. Davies, O. Liran, N. Peled, and H. Haick, "Silicon nanowire sensors enable diagnosis of patients via exhaled breath," ACS Nano **10**, 7047–7057 (2016).
[6]L. Hrachowinaa, G. Domènech-Gil, A. Pardo, M. S. Seifner, I. Gràcia, C. Cané, A. Romano-Rodríguez, and S. Barth, "Site-specific growth and in situ integration of different nanowire material networks on a single chip: Toward a nanowire-based electronic nose for gas detection," ACS Sens. **3**, 727–734 (2018).
[7]D. Marris-Morini, V. Vakarin, J. M. Ramirez, Q. Liu, A. Ballabio, J. Frigerio, M. Montesinos, C. Alonso-Ramos, X. Le, S. Serna, D. Benedikovic, D. Chrastina, L. Vivien, and G. Isella, "Germanium-based integrated photonics from near- to mid-infrared applications," Nanophotonics **7**, 1781–1793 (2018).
[8]S. Liao, N.-N. Feng, D. Feng, P. Dong, R. Shafiiha, C.-C. Kung, H. Liang, W. Qian, Y. Liu, J. Fong, J. E. Cunningham, Y. Luo, and M. Asghari, "36 GHz submicron silicon waveguide germanium photodetector," Opt. Express **19**, 10967–10972 (2011).
[9]C. Monmeyran, I. F. Crowe, R. M. Gwilliam, J. Michel, L. C. Kimerling, and A. M. Agarwal, "Strategies for increased donor electrical activity in germanium (opto-) electronic materials: A review," Int. Mater. Rev. **62**, 334–347 (2017).
[10]Z. Qi, H. Sun, M. Luo, Y. Jung, and D. Nam, "Strained germanium nanowire optoelectronic devices for photonic-integrated circuits," J. Phys. **30**, 334004 (2018).
[11]Y. J. Cho, H. S. Im, H. S. Kim, Y. Myung, S. H. Back, Y. R. Lim, C. S. Jung, D. M. Jang, J. Park, E. H. Cha, W. I. Cho, F. Shojaei, and H. S. Kang, "Tetragonal phase germanium nanocrystals in lithium ion batteries," ACS Nano **7**, 9075–9084 (2013).
[12]Y. Ikoma, T. Toyota, Y. Ejiri, K. Saito, Q. Guo, and Z. Horita, "Allotropic phase transformation and photoluminescence of germanium nanograins processed by high-pressure torsion," J. Mater. Sci. **51**, 138–143 (2016).
[13]B. D. Malone and M. L. Cohen, "Electronic structure, equation of state, and lattice dynamics of low-pressure Ge polymorphs," Phys. Rev. B **86**, 054101 (2012).
[14]D. Selli, I. A. Baburin, R. Martoňák, and S. Leoni, "Novel metastable metallic and semiconducting germaniums," Sci. Rep. **3**, 1466 (2013).
[15]A. Grüttner, R. Nesper, and H. G. V. Schnering, "Novel metastable germanium modifications allo-Ge and 4H-Ge from Li_7Ge_{12}," Angew. Chem., Int. Ed. **21**, 912–913 (1982).
[16]S. Minomura, "Pressure-induced transitions in amorphous silicon and germanium," J. Phys. Colloq. **42**, C4-181–C4-188 (1981).
[17]S. B. Qadri, E. F. Skelton, and A. W. Webb, "High pressure studies of Ge using synchrotron radiation," J. Appl. Phys. **54**, 3609–3611 (1983).
[18]F. P. Bundy and J. S. Kasper, "A new dense form of solid germanium," Science **139**, 340–341 (1963).
[19]M. Imai, T. Mitamura, K. Yaoita, and K. Tsuji, "Pressure-induced phase transition of crystalline and amorphous silicon and germanium at low temperatures," High Pressure Res. **15**, 167–189 (1996).
[20]F. Coppari, J. C. Chervin, A. Congeduti, M. Lazzeri, A. Polian, E. Principi, and A. D. Cicco, "Pressure-induced phase transitions in amorphous and metastable crystalline germanium by Raman scattering, x-ray spectroscopy, and *ab initio* calculations," Phys. Rev. B **80**, 115213 (2009).
[21]J. V. Zaikina, E. Muthuswamy, K. I. Lilova, Z. M. Gibbs, M. Zeilinger, G. J. Snyder, T. F. Fässler, A. Navrotsky, and S. M. Kauzlarich, "Thermochemistry, morphology, and optical characterization of germanium allotropes," Chem. Mater. **26**, 3263–3271 (2014).
[22]S. Sato, S. Nozaki, and H. Morisaki, "Tetragonal germanium films deposited by the cluster-beam evaporation technique," Appl. Phys. Lett. **66**, 3176 (1995).
[23]R. Nelmes, H. Liu, S. Belmonte, J. Loveday, M. McMahon, D. Allan, D. Häusermann, and M. Hanfland, "*Imma* phase of germanium at ∼80 GPa," Phys. Rev. B **53**, R2907–R2909(R) (1996).
[24]X. Chen, C. Zhang, Y. Meng, R. Zhang, H. Lin, V. Struzhkin, and H. Mao, "β−tin→Imma→sh phase transitions of germanium," Phys. Rev. Lett. **106**, 135502 (2011).

[25]A. G. Lyapin, V. V. Brazhkin, S. V. Popova, and A. V. Sapeliki, "Nonequilibrium phase transformations in diamond and zincblende semiconductors under high pressure," Phys. Status Solidi B **198**, 481–490 (1996).
[26]Y. K. Vohra, K. E. Brister, S. Desgreniers, A. L. Ruoff, K. J. Chang, and M. L. Cohen, "Phase-transition studies of germanium to 1.25 Mbar," Phys. Rev. Lett. **56**, 1944–1947 (1986).
[27]K. Takemura, U. Schwarz, K. Syassen, M. Hanfland, N. E. Christensen, D. L. Novikov, and I. Loa, "High-pressure Cmca and hcp phases of germanium," Phys. Rev. B **62**, R10603(R) (2000).
[28]C. H. Bates, F. Dachille, and R. Roy, "High-pressure transitions of germanium and a new high-pressure form of germanium," Science **147**, 860–862 (1965).
[29]B. C. Johnson, B. Haberl, S. Deshmukh, D. Brad Malone, M. L. Cohen, J. C. McCallum, J. S. Williams, and J. E. Bradby, "Evidence for the R8 phase of germanium," Phys. Rev. Lett. **110**, 085502 (2013).
[30]R. J. Nelmes, M. I. McMahon, N. G. Wright, D. R. Allan, and J. S. Loveday, "Stability and crystal structure of BC8 germanium," Phys. Rev. B **48**, 9883(R) (1993).
[31]J. D. Joannopoulos and M. L. Cohen, "Electronic properties of complex crystalline and amorphous phases of Ge and Si. I. Density of states and band structures," Phys. Rev. B **7**, 2644–2657 (1973).
[32]Z. Zhao, H. Zhang, D. Y. Kim, W. Hu, E. S. Bullock, and T. A. Strobel, "Properties of the exotic metastable ST12 germanium allotrope," Nat. Commun. **8**, 13909 (2017).
[33]L. Q. Hutson, B. C. Johnson, B. Haberl, S. Wong, J. S. Williams, and J. E. Bradby, "Thermal stability of simple tetragonal and hexagonal germanium," J. Appl. Phys. **122**, 175108 (2017).
[34]A. Mujica and R. J. Needs, "First-principles calculations of the structural properties, stability, and band structure of complex tetrahedral phases of germanium: ST12 and BC8," Phys. Rev. B **48**, 17010–17017 (1993).
[35]M. Shishkin and G. Kresse, "Self-consistent GW calculations for semiconductors and insulators," Phys. Rev. B **75**, 235102 (2007).
[36]S. J. Kim, O. K. Quy, L.-S. Chang, E. A. Stach, C. A. Handwerker, and A. Wei, "Formation of the ST12 phase in nanocrystalline Ge at ambient pressure," J. Mater. Chem. **20**, 331–337 (2010).
[37]S. Sato, S. Nazaki, and H. Morisaki, "Density of states of the tetragonal-phase germanium nanocrystals using x-ray photoelectron spectroscopy," Appl. Phys. Lett. **72**, 2460–2462 (1998).
[38]Y. Saito, "Crystal structure and habit of silicon and germanium particles grown in argon gas," J. Cryst. Growth **47**, 61–72 (1979).
[39]C. Jia, Z. Lin, Y. Huang, and X. Duan, "Nanowire electronics: From nanoscale to macroscale," Chem. Rev. **119**, 9074–9135 (2019).
[40]C. K. Chan, X. F. Zhang, and Y. Cui, "High capacity Li ion battery anodes using Ge nanowires," Nano Lett. **8**, 307–309 (2008).
[41]T. Kennedy, E. Mullane, H. Geaney, M. Osiak, C. O. Dwyer, and K. M. Ryan, "High-performance germanium nanowire-based lithium-ion battery anodes extending over 1000 cycles through *in situ* formation of a continuous porous network," Nano Lett. **14**, 716–723 (2014).
[42]F. Shen, J. Wang, Z. Xu, Y. Wu, Q. Chen, L. Xiaoguang, X. Jie, L. Li, M. Yao, X. Guo, and T. Zhu, "Rapid flu diagnosis using silicon nanowire sensor," Nano Lett. **12**, 3722–3730 (2012).
[43]S. Barth, R. Jimenez-Diaz, J. Samà, J. D. Prades, I. Gracia, J. Santander, C. Canec, and A. Romano-Rodriguez, "Localized growth and in situ integration of nanowires for device applications," Chem. Commun. **48**, 4734–4736 (2012).
[44]A. M. Chockla and B. A. Korgel, "Seeded germanium nanowire synthesis in solution," J. Mater. Chem. **19**, 996–1001 (2009).
[45]J. S. Kasper and S. M. Richards, "The crystal structures of new forms of silicon and germanium," Acta Crystallogr. **17**, 752–755 (1964).
[46]S. Bao, D. Kim, C. Onwukaeme, S. Gupta, K. Saraswat, K. H. Lee, Y. Kim, D. Min, Y. Jung, H. Qiu, H. Wang, E. A. Fitzgerald, C. T. Seng, and D. Nam, "Low-threshold optically pumped lasing in highly strained germanium nanowires," Nat. Commun. **8**, 1845 (2017).
[47]C. Adamo and V. Barone, "Toward reliable density functional methods without adjustable parameters: The pbe0 model," J. Chem. Phys. **110**, 6158–6170 (1999).
[48]A. S. Cooper, "Precise lattice constants of germanium, aluminum, gallium arsenide, uranium, sulphur, quartz and sapphire," Acta Crystallogr. **15**, 578–582 (1962).
[49]M. Balkanski, R. F. Wallis, and E. Haro, "Anharmonic effects in light scattering due to optical phonons in silicon," Phys. Rev. B **28**, 1928–1934 (1983).
[50]D. Majumdar, S. Biswas, T. Ghoshal, J. D. Holmes, and A. Singha, "Probing thermal flux in twinned Ge nanowires through Raman spectroscopy," ACS Appl. Mater. Interfaces **7**, 24679–24685 (2015).
[51]A. Cassidy, N. Tsud, S. Bercha, V. Feyer, K. C. Prince, and O. Plekan, "Adsorption of 5-Fluorouracil on Au (111) and Cu (111) surfaces," AIP Adv. **9**, 085318 (2019).
[52]R. Singha, S. Samanta, S. Chatterjee, A. Pariari, D. Majumdar, B. Satpati, L. Wang, A. Singha, and P. Mandal, "Probing lattice dynamics and electron-phonon coupling in the topological nodal-line semimetal ZrSiS," Phys. Rev. B **97**, 094112 (2018).
[53]A. D. Cicco, A. C. Frasini, M. Minicucci, E. Principi, J. Itiè, and P. Munsch, "High-pressure and high-temperature study of phase transitions in solid germanium," Phys. Status Solidi B **240**(1), 19–28 (2003).
[54]M. Omar, "Models for mean bonding length, melting point and lattice thermal expansion of nanoparticle materials," Mater. Res. Bull. **47**, 3518–3522 (2012).
[55]S. Mamand, M. Omar, and A. Muhammad, "Nanoscale size dependence parameters on lattice thermal conductivity of wurtzite GaN nanowires," Mater. Res. Bull. **47**, 1264–1272 (2012).
[56]M. Omar and H. Taha, "Lattice dislocation in Si nanowires," Physica B **404**, 5203–5206 (2009).
[57]D. S. Kim, H. L. Smith, J. L. Niedziela, C. W. Li, D. L. Abernathy, and B. Fultz, "Phonon anharmonicity in silicon from 100 to 1500 K," Phys. Rev. B **91**, 014307 (2015).